

Spectral light attenuation in Amazonian waters

Costa, M.P.F.^{1,4}, Telmer, K.^{2,3}, and Novo, E.M.L.M.⁴

¹University of Victoria, Department of Geography, Canada
PO Box 3050, Victoria, BC (maycira@office.geog.uvic.ca)

²University of Victoria, School of Earth and Ocean Sciences, Victoria, Canada

³Universidade de Campinas, São Paulo, Brazil

⁴Instituto Nacional de Pesquisas Espaciais, São Paulo, Brazil

ABSTRACT

Amazonian waters are commonly classified coarsely as white, black, and clear, reflecting their differing composition of particulate and dissolved compounds. Accordingly, the water light field and the ecology of each of these water types also differ strongly. Recent changes in land use are causing changes in river water composition that cause shifts in the water light field. Consequently, the quality and distribution of ecological habitats must also be changing. We investigate and quantify changes in the light field by reporting the first *in situ* spectral diffuse attenuation and scalar irradiance measurements and accompanying water optical constituents, including pigments determined by HPLC, from a suite of large white, black, and clear rivers of the Amazon Basin. Using this dataset, we evaluate the potential shifts in the water light field of waters affected by thousands of small-scale gold miners.

Sampling was done during the high-water period along a 500 km transect of the Amazon River and six of its larger tributaries. Water samples were collected from the subsurface and analyzed for chlorophyll *a* and other pigments, total suspended solids, and colored dissolved organic matter. At each station, vertical profiles of temperature, spectral downwelling irradiance and upwelling radiance were taken from the surface down to the depth of 1% light penetration (Z_{eu}). Our results show that, for the different types of

waters, the diffuse attenuation coefficient has different spectral and penetration depth behavior due to varying proportions of dissolved and particulate compounds. In white and black waters, the photosynthetic active radiation becomes spectrally dominated by red light as a result of the high attenuation by suspended sediments and colored dissolved organic matter, respectively. Blue radiation is non-existent below the 0.5 depth. This is not the case for clear waters, which exhibit a mid-spectra green light peak within the deep Z_{eu} , and blue light is only attenuated by 2.5 m. Applying these results to clear waters that have been muddied by the injection of sediment from mining, we show that significant changes in the distribution of spectral scalar irradiance must occur, and that this would result in a decrease (i) in photosynthetic activity, (ii) in the production of organic matter photoproducts, (iii) in the size of clear water habitats, and shifts in biological communities.

Keywords: Amazon, rivers, light attenuation, scalar irradiance, land use change

Introduction

In the Amazon, the characteristics of rainfall, the origin of the water, type of geology, soil, and vegetation occurring in the catchments produce three main types of waters (Konkauser et al., 1994), generally referred to as white, black, and clear waters (Sioli, 1950). These classes differ due to natural diversity in their concentrations of particulate and dissolved compounds (Furch and Junk, 1997). However, conversion of forest to agriculture (Williams and Melack, 1997; Neill et al., 2001; Ballester et al., 2003; Williams et al., 2004; Thomas et al., 2004) and the conversion of forest and floodplains to mining operations (Roland and Esteves, 1998; Mol and Auboter, 2003; Guenther and

Bozelli, 2004; Telmer et al., 2006) causes an increase in both physical and chemical erosion leading to increased amounts of particulate and dissolved compounds in rivers. For instance clear water lakes, such as Batata Lake in the watershed of the Trombetas River, have shown increased suspended solid concentrations up to 50 mg l^{-1} since 1979 when bauxite tailings first were discharged into the lake (Bozelli and Garrido, 2000). Mol and Ouboter (2003) have shown that streams affected by small scale gold mining in Suriname have concentrations of suspended solids up to $2,468 \text{ mg l}^{-1}$ compared to undisturbed streams, which have concentrations of about 30 mg l^{-1} . Telmer et al. (2006) have shown that since the beginning of the gold rush in the 1970s, the Creporí River in the Tapajós watershed has changed from a clear to a white water river, with present concentrations of suspended solids of up to 500 mg l^{-1} .

As a consequence, shifts in the water light field, leading to reductions in fish diversity, and switches in community structures have been reported (Mol and Ouboter, 2003), illustrating that the water light field of Amazonian waters is a critical ecological parameter. Despite its importance, remarkably few studies (Roland and Esteves, 1998) have investigated the water light field of Amazonian waters and none have spectrally resolved attenuation and available irradiance for different waters. It is of great value to do so because light is selectively attenuated by the biological community and for photochemical processes (Kirk, 1994) and therefore spectrally resolving the water light field can provide the most robust understanding of how biological and chemical processes are impacted by changes in water quality. As well, to most successfully separate human impacts from natural variations in underwater light, baseline information on the natural variations is needed.

With these needs in mind, this study's objectives were to measure the spectral diffuse attenuation and the scalar irradiance from just below the water surface down to a depth in which photosynthetic active radiation (PAR) declined to 1% (Z_{eu}) in the large black, white, and clear water rivers of the Amazon Basin. We then apply these results to clear waters that have been impacted by discharges from gold mines and discuss the probable shifts that would occur in the in-water light field and related chemical and biological processes.

Methods

Study area

Sampling was done along a 500 km E-W transect ($60^{\circ}07'W$ to $54^{\circ}08'W$) of the Amazon River beginning upstream from the Solimões and Negro confluence, to the Tapajós River, at Santarém. Samples were collected in the high-water season (June 2005) from three sections of the main stem and six major tributaries of the Amazon River. The following rivers were sampled: Solimões, Negro, Amazon (three stations), Madeira, Uatumã, Trombetas, and Tapajós (Figure 1). These rivers represent white, black, clear, and mixed-water rivers of the Amazon Basin (Table 1). The main stem samples are from locations downstream of the confluence of the Negro/Solimões, of the confluence of the Madeira, and of the confluence of the Tapajós River. The tributary samples were taken well upstream of confluences to avoid mixing with the Amazon River.

[Insert Figure 1]

Water samples

For each tributary and Amazon River stations, samples were collected at three different locations, producing 27 discrete samples. To characterize each river, the samples from

the three different locations were averaged. Water samples were collected from 0.5 m depth and analyzed for optical water constituents as follows. Water was immediately filtered onboard the boat through pre-weighed and pre-ignited GF/F 0.7 μm glass-fiber membranes to determine total suspended solids [TSS]. The filtrate was collected in amber glass bottles and kept cold and dark in coolers for later determination of absorbance due to colored dissolved organic matter (CDOM). [TSS] was determined by weight difference following methods of APHA (1998). The filtrate was analyzed spectrophotometrically for absorbance at 440nm, which was subtracted from absorbance of Milli-Q water, to determine the absorption coefficient of CDOM ($a_{\text{CDOM}} \text{m}^{-1}$) as per Kirk (1994).

Pigments were determined by High Performance Liquid Chromatography (HPLC). The following were quantified using certified standards: Chlorophyll a, b, and c (Sigma-Aldrich Canada, Inc), zeaxanthin, alloxanthin, diadinoxanthin, peridinin, and fucoxanthin (DHI Water and Environment). The HPLC procedure was based on that of EPA (1997), Mantoura and Repeta (1997), Claustre et al. (2004). In the field, water samples were vacuum filtered onto GF/F glass-fiber membranes, folded, put into custom made aluminum foil envelopes for protection from light, and then frozen. They were kept frozen by dry ice while transported to Canada. Just before HPLC analysis, the membranes were removed from the freezer, placed in centrifuge tubes with 90% acetone solution, grounded, left for 12 hours to digest while kept cold and dark, and then centrifuged to separate solids such as glass fibers and broken cell materials from the liquid pigment extract. The extracts were filtered (0.45 μm membranes) into amber auto sampler vials, and kept chilled and dark for imminent HPLC analysis. Analysis was done using a refrigerated auto sampler, an injection volume of 200 μL , and a Dionex Summit

P680A HPLC equipped with a programmable gradient pump, reverse-phase C₁₈ (5 μm pore size, 120 Å, 4.6 x 250 mm) analytical and guard columns, and a 1000 channel photodiode array UV/VIS detector.

In situ optical data collection

At each of the 27 discrete locations, optical data was acquired. Vertical profiles were acquired with a Satlantic HyperPRO set, from subsurface to Z_{eu}. The Satlantic HyperPRO set combines two in-water HyperOCR hyperspectral radiometers to measure downwelling irradiance ($E_d(z,\lambda)$) and upwelling radiance ($L_u(z,\lambda)$), and sensors for conductivity, temperature, and depth determinations. A third HyperOCR hyperspectral radiometer was installed on a pole on the top of the boat to measure above-water downwelling irradiance ($E_s(\lambda)$). All the measurements were simultaneously taken through a computer interface. These radiometers operate in a calibrated spectral range from 350 to 800 nm. All sensors were freshly calibrated by the manufacturers prior to this field experiment.

The in-water $E_d(z,\lambda)$ (180° field of view – FOV) and $L_u(z,\lambda)$ (8.5° FOV) radiometers were mounted on the same horizontal plane (T frame), with a vertical offset of 30 cm (Figure 2), which was accounted for when processing the data. The profiling set was mounted on a downrigger on the side of the boat, which was always oriented in such a way that the sensors were on the sunny side to avoid boat shading. The sensors were slowly lowered in a continuous manner to collect high vertical resolution data and to prevent significant tilt. Additional information about sun elevation, sky conditions, and wind speed were recorded for each location.

Processing of optical data

Data were filtered for tilt and synchronized with depth and time and then the diffuse attenuation coefficient ($K_d(z,\lambda)$) and scalar irradiance ($E_o(z,\lambda)$) were calculated. $K_d(z,\lambda)$ depends on (i) the inherent optical properties of the water, such as absorption and scattering coefficients and volume scattering phase function, which are a function of the properties of water, organic and inorganic suspended solids, and dissolved organic matter, and (ii) the ambient downwelling irradiance (Mobley, 1994). As such, $K_d(z,\lambda)$ is a convenient descriptor of the attenuation of light at any given depth. $K_d(z,\lambda)$ is calculated using the Lambert-Beer equation, as follows (Fergion and Mueller, 2000):

$$K_d(z,\lambda) = -1/\Delta z \times \ln[E_d(z_2,\lambda) / E_d(z_1,\lambda)] \quad (1)$$

where $E_d(z_1,\lambda)$ and $E_d(z_2,\lambda)$ are the measured downwelling irradiance at the first and second depth, respectively, and Δz is the change in depth between subsequent measurements. For these case 2 waters, we consider that the effects of solar elevation (measured between 45° and 65°) on $K_d(z,\lambda)$ are less significant than the optical composition of the water, as has been suggested in Kirk (1994), and more recently in Mishra et al. (2005).

Scalar irradiance is defined as the integral of radiance distribution from all directions around a point in the medium, and as such describes total light availability in the water (Kirk, 1994). The scalar irradiance is calculated as follows (Mobley, 1994):

$$E_o(z,\lambda) = E_{ou}(z,\lambda) + E_{od}(z,\lambda) \quad (2)$$

where $E_{ou}(z,\lambda)$ and $E_{od}(z,\lambda)$ are the spectral upward and downward scalar irradiances, respectively. $E_{ou}(z,\lambda)$ is estimated from measured $L_u(z,\lambda)$ following Kirk (1994): ($E_u \approx L_u \times 5$) and ($E_{ou} = E_u/\mu_u$), where μ_u is the average cosine of upwelling light. We assumed

a value of 0.4 throughout the euphotic zone as a good approximation of μ_u (Voss, 1989; Kirk, 1994; Mobley, 1994). $E_{od}(z,\lambda)$ is estimated from measured $E_d(z,\lambda)$ following Kirk (1994): $E_{od} = E_d/\mu_d$, where μ_d is the average cosine of downwelling light. We adopted a value of 0.7 for white waters and 0.8 for clear and black waters (Kirk, 1994). The different μ_d values are due to the increased scattering relative to absorption, as expected for white waters because of their high TSS; consequently, the underwater light becomes more diffuse and μ_d is smaller (Voss, 1989; Kirk, 1994; Mobley, 1994; Bergman et al., 2004).

Results and Discussion

Optical variability of Amazonian waters

Amazonian river waters are typically broadly categorized into three simple classes according to the color seen by an above-water observer: white, black, and clear waters (Sioli, 1950). However, not surprisingly, the in-water spectral characteristics of the light field observed in this study, and therefore the available light for biological and photochemical processes, is more diverse than this simple classification. The attenuation coefficient (K_d) and scalar irradiance (E_o) exhibit clear spectral and depth-dependencies for the different classes of water. Additionally, K_d appears to behave in a conservative manner, meaning that when waters mix, the result is the weighted sum of the parts.

a_{CDOM} , [Chla] and [TSS] at subsurface, temperature from surface up to Z_{eu} (T_{Zeu}) varied with water class – white, black, clear, and mixed waters. The low standard deviation of (T_{Zeu}) indicates that, at this period of the hydrological cycle, the depth of 1% light penetration occurs in a well-mixed layer. The rivers are vigorously flowing and

surface winds are moderate and so it is not surprising that turbulent mixing occurs throughout the relatively shallow euphotic zone. Richey et al. (1986) found similar conditions. The overall range of measured [TSS] and [Chla], 1.6 to 66.9 mg/l and 0.2 to 2.6 $\mu\text{g/l}$, respectively, are within values published in the literature for the different classes of Amazonian waters (Furch and Junk, 1997; Novo et al., 2004). Measured a_{CDOM} values range from 1.6 to 11 m^{-1} . The low and high ends of the a_{CDOM} range are observed in clear and black waters, respectively. The measured high end of a_{CDOM} is comparable to the highest reported in the literature for other regions of the world (Dekker, 1993; Kirk, 1994; Yacobi, 2003; Galegos, 2005). This is expected due to the known high concentrations of dissolved organic carbon in Amazonian black waters compared to clear and white waters (Kuchler et al., 2000; Amado et al., 2006).

[Insert Table 1]

Figure 2 shows the concentration of surface water [Chla] and diagnostic marker pigments, fucoxanthin, chl c_2 , and diadinoxanthin (from diatoms), peridinin (from dinoflagellates), alloxanthin (from cryptophytes), zeaxanthin (cyanophyceae). Pigment composition in the clear waters of the Tapajós is characterized by a high [zeaxanthin]/[Chla] ratio (0.16), indicating dominant presence of Cyanophytes. Both clear and black water rivers exhibit relatively high fucoxanthin, diadinoxanthin, and chl c_2 , indicating the presence of diatoms, and alloxanthin, indicating the presence of cryptophytes. The concentrations of the other pigments are very low, especially for white waters where they are below the detection limit. Notably, the detection limit for white waters is worse than clear or black waters because only small volumes of water can be filtered before the membranes become clogged.

[Insert Figure 2]

The measured concentrations of [TSS] and [Chla], and a_{CDOM} for the different rivers attenuate spectral light in different manners. This determines the depth of 1% light penetration (Z_{eu}), and therefore the availability of spectral scalar irradiance at a given depth. Our observations have shown that there is a two to six-fold variation of Z_{eu} for the studied waters (Table 1).

Specifically, for white waters, the Z_{eu} is the shallowest ($\cong 1$ m), while diffuse attenuation coefficients of spectral light are the highest (Figure 3 and Table 2). For these waters ($K_{dPAR} \cong 5$ m⁻¹), subsurface K_{d_B} value is $\cong 9$ m⁻¹, and decreases to $\cong 4$ m⁻¹ at Z_{eu} . These values are lower (subsurface $\cong 5$ m⁻¹ and at $Z_{eu} \cong 2$ m) for the Amazon3 location due to a mixing with the waters of the Uatumã, Trombetas and Tapajós rivers (see the attenuation balance below). Both K_{d_G} and K_{d_R} for white waters show similar trends, with more or less constant values with increasing depth, 6 m⁻¹ and 4 m⁻¹, respectively. Accordingly, K_{d_B} contributes the most to the vertical variability of K_{dPAR} (Figure 3).

The overall high attenuation in white waters is the result of (i) the highest [TSS] ($\cong 46$ mg/l) strongly scattering light in a quasi non-selective manner, thus contributing to the magnitude of attenuation in all PAR wavelengths. The source of the high-sediment load of the Amazon River is in the Andes (Konhauser et al., 1994). And (ii) the relative intermediate a_{CDOM} (5.5 m⁻¹) absorbing light in a selective manner, thus contributing to attenuation of blue wavelengths. Water molecules present high absorption in the red wavelengths, thus contributing to attenuation in this range of the spectra. Inorganic and dissolved matter have been similarly reported as dominant attenuators in several lakes of the Mackenzie Delta, where K_{dPAR} values are as high as the values observed in the

Amazon waters (Squires and Lesack, 2003), and in costal lagoons in Florida, where K_{dPAR} values are lower (Christian and Sheng, 2003). It is possible that chlorophyll is not a major attenuator of light in Amazonian white waters because of the low concentrations ($\cong 0.3 \mu\text{g/l}$). The partitioning of K_{dPAR} into attenuation by water (K_w), attenuation by CDOM (K_{CDOM}) and attenuation by particulates, Chla and TSS (K_{part}), show a first approximation of the role of the different constituents as attenuators of light (Kirk, 1994). K_w is constant and defined as 0.027 m^{-1} (Smith and Baker, 1978). K_{CDOM} is defined according to Pfanckuche (2002) as $K_{CDOM} = 0.221 \times a_{CDOM}$ (Lund-Hansen, 2004), and K_{part} is the result of subtraction the measured K_{dPAR} from ($K_w + K_{CDOM}$). This results in a 25% and 75% contribution of K_{CDOM} and K_{part} to the total K_{dPAR} , respectively (K_w is negligible at this K_{dPAR} range). Given the very low [Chla], we can confidently assume that the attenuation by particulates (K_{part}) is mostly due to [TSS].

Our study shows that light limitation due to high attenuation of spectral light, especially blue light, by inorganic and dissolved organic matter possibly prevents higher concentrations of chlorophyll *a*. Limiting nutrients may also play an important role in productivity of white waters (Putz and Junk, 1997). In these waters, blue light only exists in the first 0.5 m (Figure 4). Below this depth and up to Z_{eu} (1 m), blue light is almost nonexistent, green light is present only in very low intensities (less than 20% of the PAR light at Z_{eu}), and red light is the least absorbed and is therefore scattered up to Z_{eu} ($\cong 80\%$ of incoming PAR light at Z_{eu}) (Table 3). Thus, below 0.5 meters depth low levels of blue and green radiation indicate that the production of dissolved organic matter photoproducts is inhibited, and absorption of the available red light likely maintains any photosynthetic activity.

[Insert Figure 3]

[Insert Table 2]

In Amazonian black water rivers, such as the Negro River ($K_{dPAR} \cong 3.5 \text{ m}^{-1}$), the K_{d_B} values at surface are lower ($\cong 7 \text{ m}^{-1}$) than for white waters, and decrease considerably with depth, reaching values of $\cong 2 \text{ m}^{-1}$ at Z_{eu} (2 m). Similarly to white waters, the K_{d_G} and K_{d_R} values are roughly constant with depth, 4 m^{-1} and 2 m^{-1} , respectively (Figure 2). The high attenuation of the short wavelengths (blue and green) is mostly due to the absorption by the high content of CDOM ($a_{CDOM} \cong 10.7 \text{ m}^{-1}$) and relative higher [Chla] $\cong 1.8 \text{ } \mu\text{g/l}$ in these waters compared with white waters (Table 1). [TSS] plays a much less important role in attenuation compared with white waters, due to their lower concentrations ($\cong 3 \text{ mg/l}$). The strong role of CDOM is shown in the partitioning of K_{dPAR} . Accordingly, K_{CDOM} and K_{part} contribute with 68% and 32% to the total K_{dPAR} , respectively.

In these waters, the high attenuation of blue light by CDOM results in rapid depletion of this type of light in the first 0.5 meters depth (Figure 3). This behavior is similar to that of white waters. Albeit the extent of the euphotic layer of black waters ($Z_{eu} = 2 \text{ m}$) is twice that of white waters ($Z_{eu} = 1 \text{ m}$); that is, when the length of Z_{eu} is taken into account, blue light is absorbed much faster in black waters than in white waters. The source of high concentrations of dissolved organic matter is the low decomposition of secondary plant compounds in the highly weathered lateritic and podsolitic soils of the drainage basin of these rivers (Kuchler et al., 2000). Accordingly, waters rich in humic and fulvic acids are carried off before decomposition is completed (Forsberg et al., 1988).

The Uatumã River ($K_{dPAR} \cong 3.4 \text{ m}^{-1}$), also considered a black water river, exhibits similar Z_{eu} and slightly lower spectral coefficient of attenuation, and higher in-water spectral light intensity, when compared with the Negro River. The differences are mostly due to the lower absorption by CDOM ($a_{CDOM} = 6.4 \text{ m}^{-1}$) and higher scattering by [TSS] $\cong 12.1 \text{ mg/l}$ (the opposite behavior of the Negro River). The slightly different optical behavior of the Uatumã River is most likely because of the location where we conducted our measurements, which indicates possible mixing with the high scattering white waters flowing from the Amazon River, through the wide floodplain, and into the Uatumã River. We would only be able to measure non-mixed black waters in locations at least 40 km upstream of where we measured.

Generally, for the black water, the scalar irradiance at Z_{eu} becomes monochromatic with total dominance of red light (96% and 86% of PAR at Z_{eu} , respectively) (Figure 4 and Table 3). In the Uatumã River, some green light is available at Z_{eu} (14% of the total PAR at Z_{eu}) compared to the Negro River (Table 3). This suggests that the inhibition of photochemical processes that use blue and green light is likely more pronounced in black waters than in white waters, and any photosynthetic activity relies on absorption of red light. Generally, very little is known about the distribution of phytoplankton species in Amazonian waters; however, in black waters diatoms (*Melosira granulata*) dominate (Puntz and Funk, 1997). To confirm this, our HPLC measurements of pigments show the presence of fucoxanthin, chl c_2 , and diadinoxanthin, which are diatoms diagnostic marker pigments, in both the Negro and the Uatumã waters (Figure 2). Diatoms have pigments that absorb radiation broadly in the blue and red spectra (chlorophylls) and the blue and green spectra (carotenoids). This less light-selective

group of phytoplankton may take advantage of the limited spectra of red light or possibly develop some ontogenic adaptation of the photosynthetic apparatus (Kirk, 1994).

[Insert Figure 4]

The Tapajós River ($K_{dPAR} = 1 \text{ m}^{-1}$), a typical clear-water river, shows the most dissimilar results in regard to Z_{eu} (5.6 m), spectral coefficient of attenuation (Figure 2) and scalar irradiance (Figures 3) compared with the white and black waters. In these clear waters the K_{d_B} values at subsurface (2 m^{-1}) and at Z_{eu} (1 m^{-1}) are the lowest among all the sampled rivers, and lower K_{d_G} and K_{d_R} are also observed (0.8 m^{-1}) (Figure 3). This is a result of the low influence of TSS (1.6 mg/l) as a scatter of spectral light, and relative low absorption of blue and green spectra by CDOM ($a_{CDOM} = 1.6 \text{ m}^{-1}$), and the selective light absorption by chlorophyll ([Chla] = 2.1 $\mu\text{g/l}$) at the blue and red spectra. The headwaters of the Tapajós River are in the stable Brazilian shield, where the weathering rates are not as strong as those occurring in the Andes. This shield is associated with clay latossol soils, which promote complete mineralization of the organic matter. Consequently, these waters have generally low concentrations of suspended solids and dissolved organic matter (Walker, 1990).

The partitioning of K_{dPAR} shows that K_{CDOM} and K_{part} contribute with 32% and 65%, respectively. Given the low [TSS], we can assume that [Chla] plays a major role in the attenuation of light in these waters. The opposite is observed in black and clear waters. In these waters, phytoplankton is therefore the dominant attenuator of light, followed by CDOM. Similar dominance of phytoplankton as an attenuator has been reported from costal waters of Denmark (Lund-Hansen, 2004) and costal lagoons in

Florida (Christian and Sheng, 2003) where K_{dPAR} is approximately the same as our measurements.

As a result of the lowest spectral K_d values, clear waters show the highest spectral scalar irradiance in the euphotic layer (Figure 3). Thus exhibiting a shift from the red-dominant light field observed in white and black waters to a green-dominant (54% of PAR reaching Z_{eu}) light field observed in the clear waters of the Tapajós River. In these waters, both diatoms and Cyanophyceae occur (Putz and Junk, 1997). Our HPLC measurements of pigments confirm this. The results show the presence of fucoxanthin, chl c_2 , and diadinoxanthin, which are diatoms diagnostic marker pigments, and zeaxanthin, a Cyanophyceae diagnostic marker pigment. Cyanophyceae likely take advantage of the higher intensity of green light in these waters because of the presence of phycocyanine photosynthetic pigment, which absorbs blue and green light. Similar behaviors in different groups of algae have been observed in the Great lakes (Bergmann et al., 2004).

The Trombetas River ($K_{dPAR} = 2 \text{ m}^{-1}$), also considered a clear water river, shows lower Z_{eu} (2.9 m), higher coefficient of attenuation (Figure 2), and lower spectral light intensity at any depth when compared with the Tapajós River. These differences are probably a result of where we conducted our measurements, and indicate a possible mixing with white waters flowing from the Amazon River, through the floodplain and into the Trombetas River. Consequently, much higher CDOM values ($a_{CDOM} \cong 4.7 \text{ m}^{-1}$) and slightly higher [TSS] = 3.3 mg/l are observed in these waters. When combined, these variables contribute to a higher K_d in the blue and green spectra (Figure 2), thus leaving

red light to penetrate deeper into the euphotic layer (81% of PAR reaching Z_{eu}), similar to that of the white waters (Table 3).

[Insert Table 3]

The conservative behavior of the diffuse attenuation coefficient: “attenuation balance”

As previously shown, K_{dPAR} values vary in a conservative manner, with the highest values observed in white waters, followed by black and clear waters, as a result of dominant attenuation by TSS, CDOM, and Chla, respectively. Given that these constituents can be represented as fluxes from the different rivers, we expect that K_{dPAR} follow the same behavior. We are calling this “attenuation balance”. For instance, using the flux of water from the Negro River (28400 m³/s) multiplied by its K_{dPAR} (3.5 m⁻¹) + the flux of water from the Solimões River (103 m³/s) multiplied by its K_{dPAR} (4.9 m⁻¹) is equal to the flux of water at Amazon1 (124000 m³/s) multiplied by its K_{dPAR} . The calculated K_{dPAR} is 4.9 m⁻¹; i.e., very close to the measured $K_{dPAR} = 5.1$ m⁻¹ at that stretch of the Amazon (Amazon1) (K_{dPAR} values are in Table 2 and discharges of rivers are in Figure 2). Similar calculations resulted in a K_{dPAR} of 4.6 m⁻¹ at location Amazon2 (measured value of 4.8 m⁻¹) after the confluence with the Madeira River, and 4.2 m⁻¹ at location Amazon3 (measured value of 4.6 m⁻¹) after the confluence with the Uatumã, Trombetas and Tapajós Rivers.

The similarity between calculated and measured K_{dPAR} for the different sections of the Amazon River suggests that K_{dPAR} is behaving conservatively such that proportions of mixing of the inputs predict the attenuation coefficient of the mix. From this, we estimate the contribution of the K_{dPAR} from each tributary to the Amazon River. The K_{dPAR} of the Negro and Solimões rivers contribute with 16.0 % and 84.0 % to the

K_{dPAR} in Amazon1, respectively. Clearly, the highly attenuated waters of the Solimões River dominate due to the high K_{dPAR} and a discharge almost four times higher than that of the Negro River. The K_{dPAR} values from Amazon1 and Madeira River contribute with 76.0 % and 24.0 % to the K_{dPAR} at location Amazon2, respectively. In this case, even with a relatively lower discharge, the Madeira River plays an important role because of its very high K_{dPAR} (the highest measured among all the rivers). Finally, the K_{dPAR} from Amazon2, Uatumã, Trombetas, and Tapajós contribute with 96.0 %, 1.0 %, 1.1 %, and 1.6 % to the K_{dPAR} at location Amazon3, respectively. Here, the combination of high discharge and high attenuation coefficient at the location Amazon2 dominates the final K_{dPAR} at Amazon3. The contribution of the low attenuation coefficient of the Tapajós River is insignificant due to the relatively low discharge from this river.

How do these findings can be applied to understanding the potential impact of small-scale gold mining on the light field of impacted waters in the Amazon Basin?

The answer to this question first requires a better understanding of the in-water light field of the Amazonian rivers in their natural states. In this study, we are providing, for the first time, this key piece of information (above). How the light field might change as a consequence of land-use changes such as mining activity has yet not been investigated. We can illustrate these possible changes by using the Tapajós River as a case study.

The Tapajós River Basin has been suffering stress of mining activity for placer gold since the 1950s; as a result, high concentrations of clay sediment have been injected into the river and transported long distances. Concentrations of suspended solids in the Tapajós River upstream of the confluence of the heavily mined Creparí River are about 7 mg/l. The Creparí River, which once was a clear water river, presently has suspended

solids concentrations of up to 500mg/l (Telmer et al., 2006). As shown in Figure 5 (Landsat TM satellite imagery), there is a strong and spreading sediment plume from the Creparí into the Tapajós waters. This sediment plume is diluted as it mixes with the Tapajós waters.

[Insert Figure 5]

To estimate the concentration of TSS in the Tapajós River downstream ($[TSS]_{Td}$) the confluence with the Creparí River, a mass balance approach is applied:

$$(Q_c \times [TSS]_c) + (Q_{Tu} \times [TSS]_{Tu}) = (Q_{Td} \times [TSS]_{Td}) \quad (3)$$

where Q_c , Q_{Tu} , and Q_{Td} are discharges from the Creparí (700 m³/s), Tapajós upstream the Creparí confluence (6256 m³/s), and Tapajós downstream the confluence with the Creparí (846805 m³/s), respectively. $[TSS]_c$, $[TSS]_{Tu}$, and $[TSS]_{Td}$ are the TSS concentrations in the Creparí (500 mg/l), Tapajós upstream (7 mg/l), and Tapajós downstream the confluence with the Creparí, respectively. The Tapajós downstream position is located about 150 km north of the confluence with the Creparí River. In solving the $[TSS]_{Td}$, we find a concentration of 47mg/l. With this high $[TSS]$, the expected changes in the intensity and spectral characteristics of the in-water scalar irradiance are extensive.

To illustrate this, we use the light patterns we directly observed with our field data. Figure 6 shows the subsurface (0.5 m depth) scalar irradiances (blue, green, and red spectra) for a clear water river (TSS = 2 mg/l; $a_{CDOM} = 1.6 \text{ m}^{-1}$; $Z_{eu} = 6 \text{ m}$) and a white water river (TSS = 41 mg/l; $a_{CDOM} = 6.9 \text{ m}^{-1}$; $Z_{eu} = 1 \text{ m}$), which are used in this case to represent Tapajós waters upstream the confluence with the Creparí, and affected Tapajós waters after the confluence with the Creparí, respectively. Therefore, increases in the

inputs of particulate and dissolved compounds into clear waters, such as the Tapajós River, results in a six-fold decrease of the euphotic layer, a significant decrease in the intensity of spectral light at subsurface, and a shift from a dominant green light field to a red light field in the euphotic layer (Figure 6). Without question these changes would alter photosynthetic activity, production of organic matter photoproducts, and possible decrease in the ecological habitat and shifts of biological communities. This scenario suggests that significant changes in the in-water light field of the Tapajós River are already occurring; therefore primary productivity is already affected and further effects, such as reduction of fish diversity and shifts in community structure, can be expected, as has been reported for other regions of the Amazon (Mol and Ouboter, 2003).

[Insert Figure 6]

Summary and Conclusion

Our results show that in the shallow euphotic layer of white and black waters photosynthetic active radiation becomes spectrally dominated by red light (80 % and 96% of PAR at Z_{eu} , respectively). This is the effect of high attenuation by suspended sediments (75% of K_{dPAR}) and colored dissolved organic matter (68% of K_{dPAR}) on the quantity and spectral quality of the light field in white and black waters, respectively. In these waters, suspended sediments attenuate light in a non-selective spectral manner, and dissolved matter selectively attenuates mostly blue light. Hence, blue radiation is non-existent below the 0.5 depth. This implies that high attenuation of blue light by CDOM controls penetration of photosynthetic radiation in these waters, and is therefore limiting productivity. Absorption of available red light likely maintains any photosynthetic

activity at Z_{eu} . This may account for the presence of diatoms, which contain pigments that broadly absorb light within the PAR range.

Conversely, clear waters are characterized by the presence of Cyanophyceae, which is likely taking advantage of available green light in the deeper euphotic layer of these waters. Different from black and white waters, in clear waters green light dominates the euphotic layer (54% of the PAR reaching Z_{eu}) as a result of the relatively smaller attenuation coefficient at this part of the spectra, and the spectrally selective attenuation by chlorophyll (roughly 65% of the total K_{dPAR}).

The attenuation of light in the waters of the Amazon River itself is a result of the mixing of fluxes of optical constituents from the tributaries. We represent the mixing of fluxes from the different rivers through an “attenuation balance.” This approach reveals that the attenuation coefficient behaves in a conservative manner such that proportions of mixing of the inputs predict the attenuation coefficient of the mix. The implication is that a combination of high discharge and/or highly attenuated waters such as those of the Solimoes and Madeira Rivers will be the strongest controls on the light field of the Amazon River.

We go on to show how these findings can be applied to understanding the potential impact of small-scale gold mining on the light field of impacted waters. Although our data only allowed us to hypothesize about potential changes in the impacted rivers, we are confident that by using the light patterns we directly observed with our field data, we have produced a reasonably accurate “best possible estimate” of impacts for these very remote regions. This estimate suggests that an injection of particulate and dissolved compounds from gold mining into clear waters like those of the

Tapajos River results in a six-fold decrease in the thickness of the euphotic layer, a significant decrease in the quantity of spectral light at any depth, and a shift from a green dominant to a red dominant light field in the euphotic layer. A physical forcing such as this would cause substantial decreases in changes in photosynthetic activity, in the production of organic matter photoproducts, and in the size of the natural habitat, all leading to strong shifts in biological communities. Although we have not yet quantified ecological changes, it surely occurs as has been shown by the studies showing decreases in phytoplankton (Guenther and Bozelli, 2004) and fish diversity (Mol and Outober, 2003) in impacted waters.

Other types of land-use change occurring in the Amazon, such as the conversion of forest into pastureland or soy plantations would also impact the distribution of light in the water, albeit the dynamics and attenuation may be different due to different seasonal and mineralogical forcings. We are not aware of any research investigating this problem, however, it has been shown that streams impacted by this type of land-use change do experience increases in particulate and inorganic matter (Neill et al., 2001; Ballester et al., 2003; Thomas et al., 2004). Given the estimated deforestation rates in the Amazon, 19,000 km²/year from 1997 to 2003, and that the rate is expected to grow (INPE, 2004), increases in the input of organic and inorganic matter are undoubtedly already occurring throughout the Basin, and these must be driving changes in the water light field and ecology – but to an unknown degree and unknown character and endpoint. We hope that by providing baseline data, which future work can employ, and by providing scenarios and insights on the impacts of human disturbances to the light field of Amazonian waters,

the degree and character of changes can be better understood, and the endpoint managed to minimize ecological damage.

References

- Amado, A.M.; Farjalla, V.F.; Esteves, F.A.; Bozelli, R.L.; Roland, F.; Enrich-Past, A. (2006). Complementary pathways of dissolved organic carbon removal pathways in clear-water Amazonian ecosystems: photochemical degradation and bacterial uptake. *FEMS Microbial Ecology*, 56: 8-17.
- APHA. (1998). *Standard Methods for the Examination of Water and Wastewater*, 1015 15th Street, NW, Washington, DC 20005.
- Ballester, M.V.R.; Victoria, D.C.; Krusche, A.V.; Coburn, R.; Victoria, R.L.; Richey, J.E.; Logsdon, M.G.; Mayorga, E.; Matricardi, E. (2003). A remote sensing/GIS-based physical template to understand the biogeochemistry of the Ji-Parana River basin (Western Amazonia). *Remote Sensing of the environment*, 87: 429-445.
- Bergmann, T.; Fahnenstiel, G.; Lohrenz, S.; Millie, D.; Schofield, O. (2004). Impacts of a recurrent resuspension event and variable phytoplankton community composition on remote sensing reflectance. *Journal of geophysical Research*. Vol. 109, C10S15.
- Bozelli, R.L.; Garrido, A.V. (2000). Gradient of inorganic turbidity and responses to planktonic communities in an Amazonian lake, Brazil. *Verhandlungen der Internationale Vereinigung für Limnologie*, 27:147-151.
- Christian, D.; Sheng, P.Y. (2003). Relative influence of various water quality parameters on light attenuation in Indian River lagoon. *Estuarine, Coastal and Shelf Science*. 57: 961-971.
- Claustre et al. (2004). *An intercomparison of HPLC phytoplankton pigment methods using in situ samples: application to remote sensing and database activities*. *Marine Chemistry* 85, 41-61.
- Dekker, A.G. (2003). Detection of optical water quality parameters for eutrophic waters by high resolution remote sensing. Ph.D. Thesis. 222p.
- EPA (1997). Method 447.0, Determination of chlorophyll a and b and identification of other pigments of interest in marine and freshwater algae using high performance liquid chromatography with visible wavelength detection. 20 pp.
- Fargion, G.S. and Mueller, J.L.(Eds). (2000). *Ocean Optics Protocols For Satellite Ocean Colour Sensor Validation, Revision 2*. National Aeronautical and Space Administration, Greenbelt, Maryland.
- Forsberg, B.R.; Devol, A.H.; Richey, J.E.; Martinelli, L.A.; Santos, H. (1988). Factors controlling nutrient concentrations in Amazon floodplain lakes, *Limnology and Oceanography*, 33(1):41-56.
- Furch, B; Otto, K. (1987). Characterization of light regime changes (PAR) by irradiance reflectance in two Amazonian water bodies with different physico-chemical properties. *Arch Hydrobiology*. 110(4):579-587.
- Furch, K.; Junk, J.W. (1997). Physicochemical Conditions in Floodplains. In: *The Central Amazon Floodplain*. Junk (Ed.), Springer-Verlag, Berlin. 525p.
- Gallegos, C.L. (2005). Optical water quality of a blackwater river estuary: the lower St. Johns River, Florida, USA. *Estuarine, Coastal and Shelf Science*, 63: 57-72.

- Guenther, M.; Bozelli, R. (2004). Effects of inorganic turbidity on the phytoplankton of an Amazonian Lake impacted by bauxite tailings. *Hydrobiology*. 511: 151-159.
- Instituto Nacional de Pesquisas Espaciais (INPE). (2004). Monitoramento da Floresta Amazonica Brasileira por satélite. Projeto PRODES (www.dpi.inpe.br/podesdigital).
- Kirk, J.T.O. (1994). *Light and Photosynthesis in Aquatic Systems*. New York: Cambridge University Press, pp. 509.
- Konhauser, K.O.; Fyfe, W.S.; Kronberg, B.I. (1994). Multi-element chemistry of some Amazonian waters and soils. *Chemical Geology*. 111:155-175.
- Kuchler, I. L.; Miekeley, N.; Forsberg, B.R. (2000). A contribution to the chemical characterization of rivers in the Rio Negro Basin, Brazil. *J. Braz. Chem. Soc.* 11(3):286-292.
- Lund-Hansen, L.C. (2004). Diffuse attenuation coefficients $K_d(\text{PAR})$ at the estuarine North-sea-Baltic Sea Transition: time-series, partitioning, absorption, and scattering. *Estuarine, Coastal and Shelf Science*, 61: 251-259.
- Mishra, D.R.; Narumalani, S.; Rundquist, D.; Lawson, M. (2005). Characterizing the vertical diffuse attenuation coefficient for downwelling irradiance in coastal waters: implications for water penetration by high resolution satellite data. *ISPRS Journal of Photogrammetry & Remote Sensing*, 60: 48-64.
- Mobley, C.D. (1994). *Light and Water - Radiative Transfer in Natural Waters*. San Diego: Academic Press Inc, pp. 592.
- Mol, J.H., Ouboter, P.E. (2003). Downstream effects of erosion from small-scale gold mining on the instream habitat and fish community of a small neotropical rainforest stream. *Conservation Biology*. 18(1):201-214.
- Neill, C.; Deegan, L.A.; Thomas, S.M.; Cerri, C.C. (2001). Deforestation of pasture alters nitrogen and phosphorus in small Amazonian streams. *Ecological Applications*. 11(6): 1817-1828.
- Novo, E.M.L.M; Pereira Filho, W.; Melack, J.M. (2004). Assessing the utility of spectral band operators to reduce the influence of total suspended solids on the relationship between chlorophyll concentration and the bidirectional reflectance factor in Amazon waters. *International Journal of Remote Sensing*. 25(22): 5105-5116.
- Putz, R.; Junk, W.J. (1997). Phytoplankton and Periphyton. In *The Central Amazon Floodplain: Ecology of a Pulsing System*, edited by W.J. Junk (Berlin: Springer), pp. 147-181.
- Richey, J.E.; Meade, R.H.; Slati, E.; Devol, A.H.; Nordin, C.F.; Santos, U. (1986). Water discharge and suspended sediment concentrations in the Amazon River:1982-1984. *Water Resources Researcher*. 22(5):756-764.
- Roland, F.; Esteves, F.A. (1998). Effects of bauxite tailing on PAR attenuation in an Amazonian crystalline water lake. *Hydrobiology*. 377:1-7.
- Sioli, H. (1950). Das wasser im Amazonasgebiet. *Forsch Fortschr*. 26:274-280.
- Smith, R.; Baker, K.S. (1978). The bio-optical state of the ocean waters and remote sensing. *Limnology and Oceanography*, 23: 247-259.
- Squires, M.M.; Lesack, F.W.L. (2003). Spatial and tempoaral patterns of light attenuation among lakes of the Mackenzie Delta. *Freshwater Biology*. 43: 1-20.
- Telmer K., Costa M.P.F., Angélica R.S., Araujo E.S., and Maurice Y. (*in press*) Mining Induced Emissions of Sediment and Mercury in the Tapajós River Basin Pará,

Brazilian Amazon, 1985-1998, determined from the Ground and from Space. *Journal of Environmental Management*.

- Thomas, S.M.; Neill, C.; Deegan, L.A.; Krusche, A.V.; Ballester, V.M.; Victoria, R.L. (2004). Influences of land use and stream size on particulate and dissolved materials in a small Amazonian stream network. *Biogeochemistry*, 68: 135-151
- Voss, K.J. (1989). Use of the radiance distribution to measure the optical absorption coefficient in the ocean. *Limnology and Oceanography*, 34(8): 1614-1622.
- Walker, I. (1990). Ecologia e biologia dos igapós e igarapés. *Ciência Hoje*, 11(64):44-53.
- Williams, M.R.; Filoso, S.; Lefebvre, P. (2004). Effects of land-use change on solute fluxes to floodplain lakes of the central Amazon. *Biogeochemistry*, 68: 259-275.
- Yacobi, Y.Z.; Alberts, J.J.; Tacaks, M.; Mcelvaine, M. (2003). Absorption spectroscopy of colored dissolved organic carbon in Georgia (USA) rivers: the impact of molecular size distribution. *Journal of Limnology*, 62(10): 41-46.

List of Figures

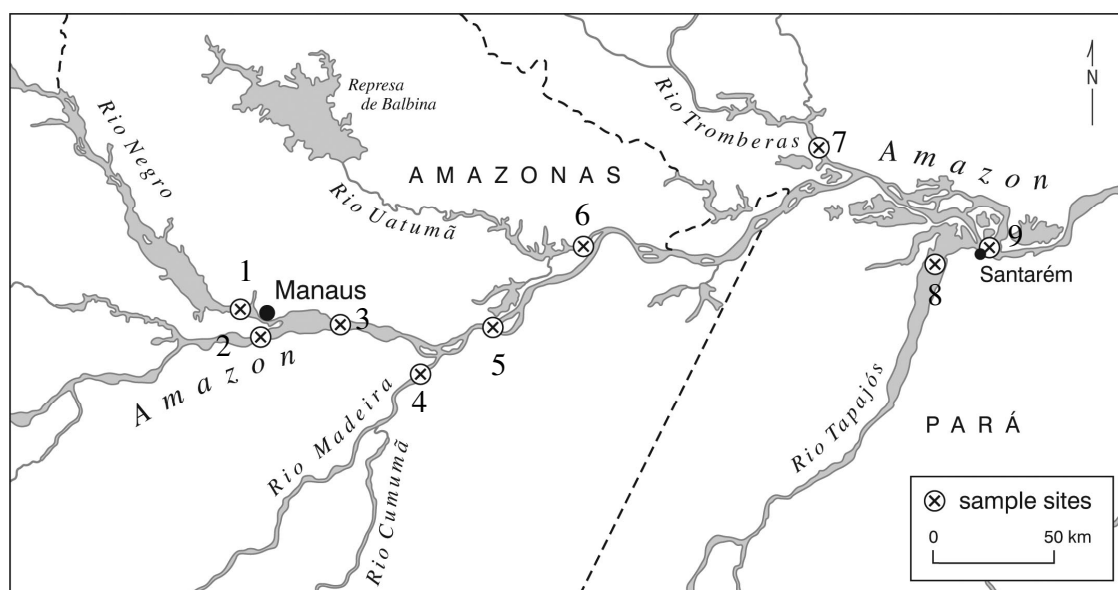
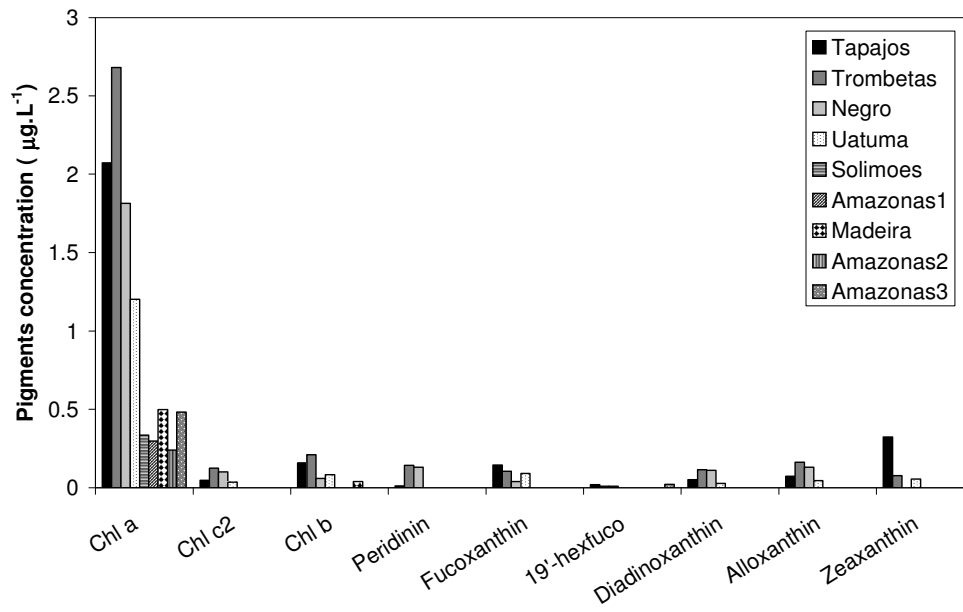


Figure 1. Sampling locations on the Amazon River and its major tributaries. Mainstem sampling regions are called Amazon1 (3), Amazon2 (5), and Amazon3 (9). Tributaries are: Negro River (1), Solimões River (2), Madeira River (4), Uatumã River (6), Trombetas River (7), and Tapajós River (8).

Figure 2. Concentration of pigments ($\mu\text{g/l}$) determined by HPLC.



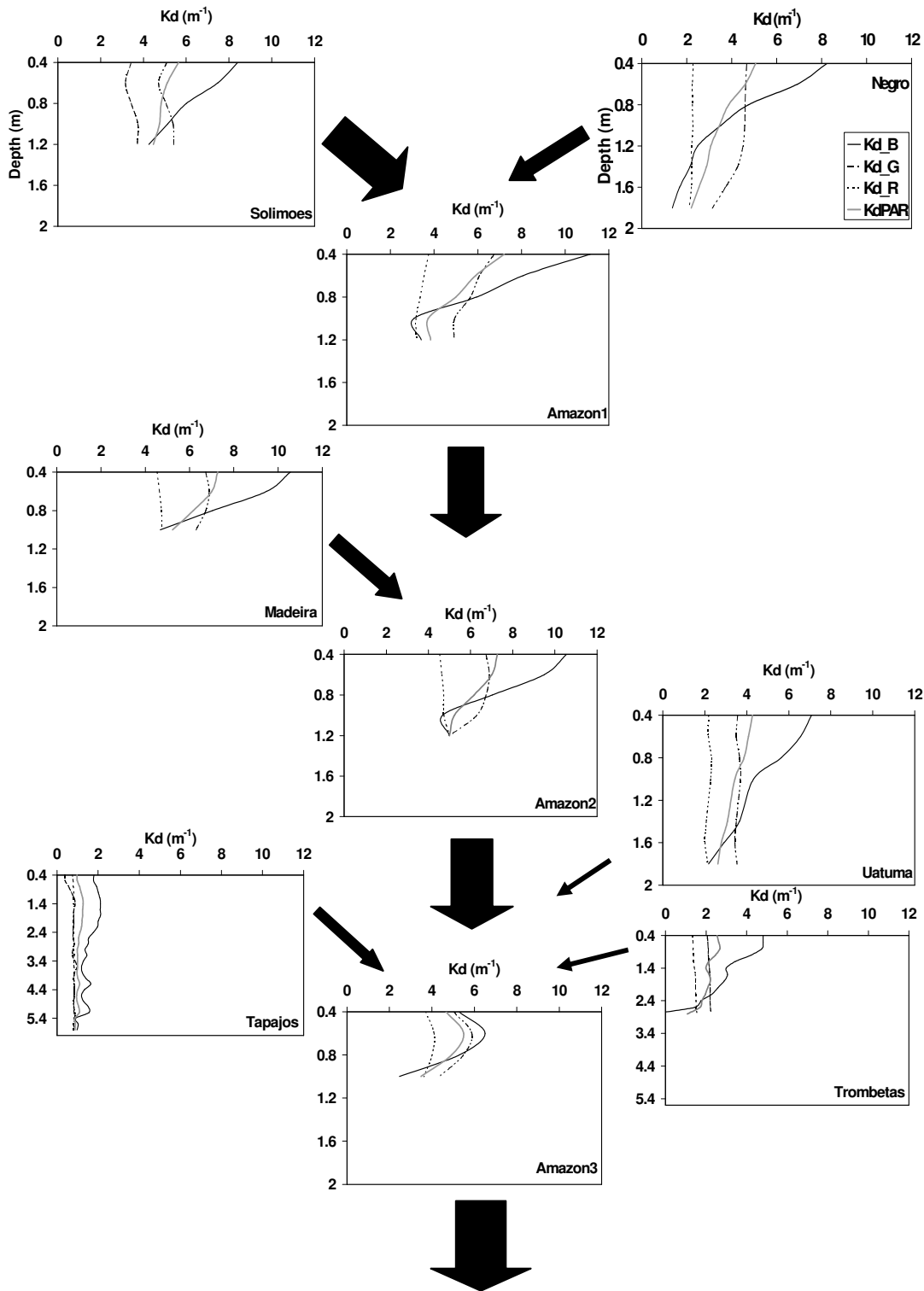


Figure 3. Vertical attenuation coefficient for the different rivers. $K_{d,B}$ (blue); $K_{d,G}$ (green); $K_{d,R}$ (red); $K_{d,PAR}$ (400-700nm). Arrows represent the direction of flow of the rivers; thickness of arrows represents discharge relative to the discharge at Amazon3. Negro ($28400\text{m}^3/\text{s}$); Solimões ($103000\text{ m}^3/\text{s}$); Amazon1 ($124000\text{ m}^3/\text{s}$); Madeira ($31200\text{ m}^3/\text{s}$); Amazon2 ($180000\text{m}^3/\text{s}$); Uatumã ($2500\text{ m}^3/\text{s}$); Trombetas ($4600\text{ m}^3/\text{s}$); Tapajós ($13500\text{ m}^3/\text{s}$); and Amazon3 ($213884\text{ m}^3/\text{s}$).

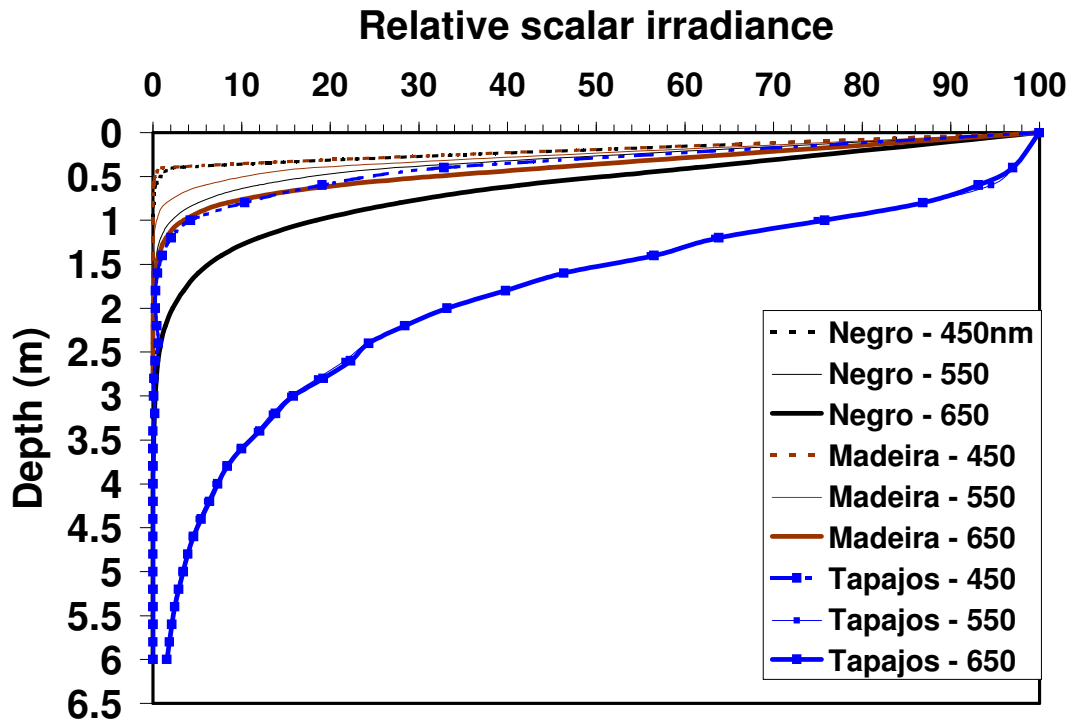


Figure 4. Scalar irradiance profiles relative to irradiance incident just below the water surface for black, white and clear waters at blue (450nm), green (550), and red (650) wavelengths. (Black (Negro; $K_{dPAR} = 4 \text{ m}^{-1}$), white (Madeira; $K_{dPAR} = 6 \text{ m}^{-1}$), and clear (Tapajos; $K_{dPAR} = 1 \text{ m}^{-1}$).

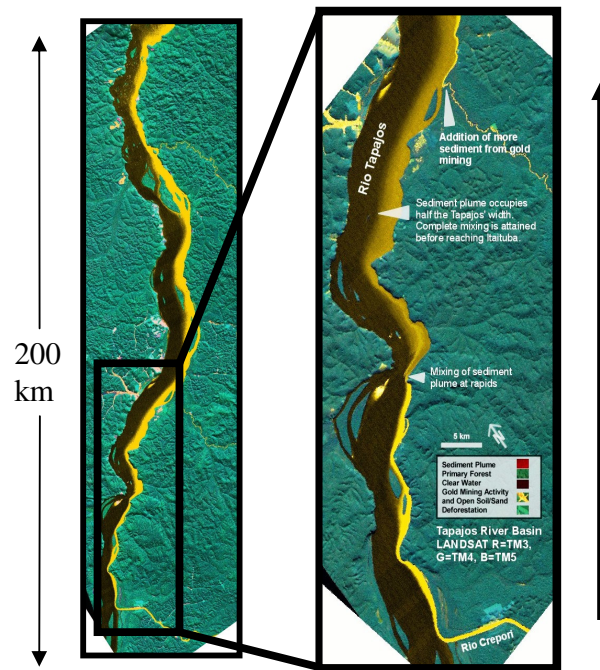


Figure 5. Landsat TM image from 1997 showing the Creporí plume discharging its mining-induced sediment load into the Tapajós River. R(TM3); G (TM4); B (TM5). Arrow represents direction of flow of the Tapajós River. From: Telmer et al., (2006).

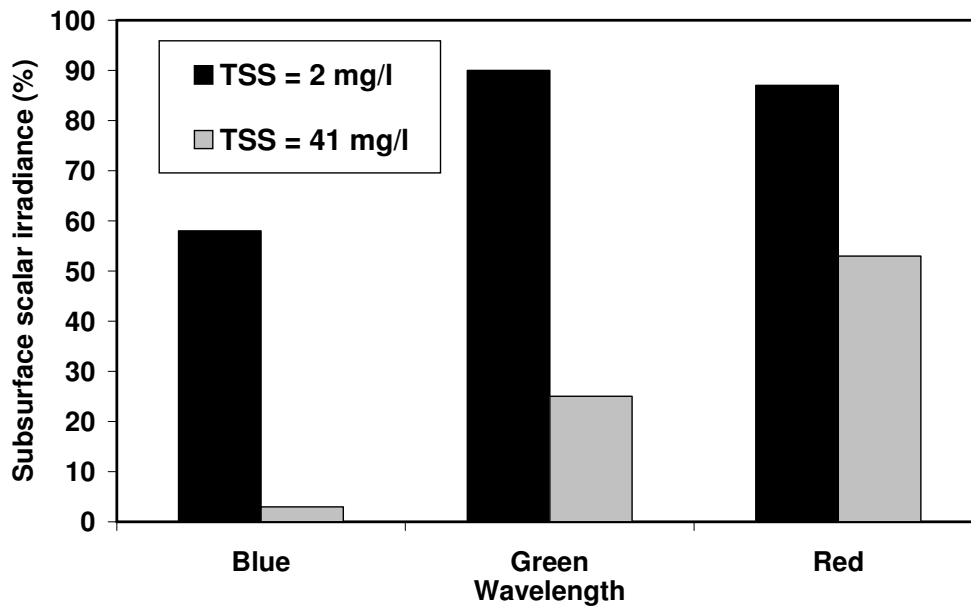


Figure 6. Changes in subsurface spectral scalar irradiance relative to irradiance just below the water surface for a non-impacted the Tapajós River with [TSS] of 2 mg/l (black bars) and a possible impacted Tapajós River with [TSS] of approximately 41 mg/l (gray bars) downstream confluence with the heavily mined Creparí River.

List of Tables

Table 1. Limnological data. Values represent mean of triplicates. Value between brackets right below the mean represents 1 standard deviation of the mean; values between brackets right below the standard deviation of the mean (only for T_{zeu}) represents mean standard deviation of vertical profile.

Rivers (region code)	Water class	Chla ($\mu\text{g/l}$)	TSS (mg/l)	a_{CDOM} (m^{-1})	Z_{eu} (m)	T_{zeu} ($^{\circ}\text{C}$)	Sun elevation (degrees)	Wind (m/s)
Negro (1)	Black	1.8	3.2	10.7 (0.2)	1.9 (0.1)	29.5 (0.22) (0.16)	75	2.5
Solimões (2)	White	0.3	66.9 (37.2)	5.1 (0.4)	1.1 (0.1)	29.7 (0.01)	60	1
Amazon1 (3)	White- mix	0.3	17.8	12.4	1.2 (0.0)	29.5 (0.004)	50	4
Madeira (4)	White	0.5	53.3 (2.2)	4.1 (0.9)	0.9 (0.1)	30.6 (0.005) (0.006)	55	2.5
Amazon2 (5)	White- mix	0.2	41.1	6.9	1.1 (0.1)	30.01 (0.07) (0.07)	42	2
Uatumã (6)	Black	1.2	12.1 (2.52)	6.4 (0.3)	1.9 (0.1)	29.9 (0.2) (0.03)	60	3
Trombetas (7)	Clear	2.7	3.3 (0.25)	4.7 (0.5)	2.9 (0.2)	29.6 (0.3) (0.3)	60	2
Tapajós (8)	Clear	2.1	1.6	1.6 (0.1)	5.6 (0.5)	30.6 (0.02) (0.04)	60	2
Amazon3 (9)	White	0.5	53.4	5.9	1.0 (0.0)	30.4 (0.02) (0.004)	45	2

Table 2: Values represent mean of triplicates K_d within the euphotic layer for the spectral range of blue (K_{d_B}), green (K_{d_G}), red (K_{d_R}), and PAR. Values between brackets right below the mean represent 1 standard deviation of the mean.

Rivers	K_{d_B} (m^{-1})	K_{d_G} (m^{-1})	K_{d_R} (m^{-1})	K_{dPAR} (m^{-1})
Negro	3.9 (2.5)	4.3 (0.6)	2.2 (0.1)	3.5 (1.0)
Solimões	6.3 (1.7)	5.1 (0.3)	3.5 (0.3)	4.9 (0.4)
Amazon1	6.3 (3.4)	5.7 (0.8)	3.4 (0.2)	5.1 (1.5)
Madeira	7.9 (2.6)	6.7 (0.3)	4.7 (0.1)	6.4 (0.9)
Amazon2	5.5 (2.8)	5.4 (0.4)	3.6 (0.1)	4.8 (1.1)
Uatumã	4.6 (1.8)	3.6 (0.1)	2.2 (0.1)	3.4 (0.6)
Trombetas	2.9 (1.6)	2.2 (0.1)	1.4 (0.1)	2.2 (0.5)
Tapajós	1.6 (0.4)	0.8 (0.1)	0.8 (0.0)	1.1 (0.1)
Amazon3	4.9 (1.7)	5.2 (0.7)	3.9 (0.2)	4.6 (0.8)

Table 3. Values represent the integral of scalar irradiance ($\mu\text{W}/\text{cm}^2$) for spectral PAR, blue, green, and red ranges, at subsurface (0.5 m) and at Z_{eu} . Values between brackets represent the percentage of the spectral energy (B, G, R) in relation to the total amount (PAR) reaching the specific depth.

River	$E_{oPAR\ 0.5}$	$E_{o\ B0.5}$	$E_{o\ Bzeu}$	$E_{o\ G0.5}$	$E_{o\ Gzeu}$	$E_{o\ R0.5}$	$E_{o\ Rzeu}$
Negro	10931.0	480.1 (4.4)	0.6 (0.3)	3532.0 (32.3)	8.6 (3.9)	6918.0 (63.3)	212.0 (95.8)
Solimoes	8619.0	428.0 (4.9)	2.6 (0.5)	3008.0 (34.9)	99.0 (19.5)	5184.0 (60.1)	407.6 (80.0)
Amazon1	9585.0	299.0 (3.1)	1.1 (0.2)	3017.0 (31.5)	54.0 (9.8)	6268.0 (65.4)	496.0 (89.9)
Madeira	7182.0	216.0 (3.0)	2.1 (0.5)	2323.0 (32.0)	81.9 (18.9)	4642.0 (64.6)	347.0 (80.5)
Amazon2	9638.0	535.0 (5.6)	2.9 (0.6)	3299.0 (34.0)	76.0 (16.0)	5804.0 (60.2)	396.0 (83.4)
Uatuma	17711.0	1205.0 (6.8)	1.7 (0.3)	6455.0 (36.5)	75.0 (13.6)	10051.0 (56.7)	474.0 (86.0)
Trombetas	26550.0	3721.0 (14.0)	0.6 (0.2)	10684.0 (40.0)	77.0 (19.0)	12145.0 (46.0)	324.0 (81.0)
Tapajos	46438.0	11561.0 (24.9)	17.8 (1.0)	18417.0 (39.7)	396.0 (54.0)	16462.0 (35.0)	324.0 (44.0)
Amazon3	4855.0	425.0 (8.8)	52.0 (10.2)	1692.0 (34.8)	121.0 (23.9)	2738.0 (56.0)	334 (65.9)